

# **Uniaxial strain parallel to impulse propagation in cultured mouse and rat cardiomyocyte strands slows conduction more than strain in the perpendicular direction**

Andrea Buccarello<sup>1</sup>, Michela Azzarito<sup>1</sup>, Frédéric Michoud<sup>2</sup>, Stéphanie P. Lacour<sup>2</sup>, Jan P. Kucera<sup>1</sup>

This is the pre-peer reviewed version of the following article: “Uniaxial strain of cultured mouse and rat cardiomyocyte strands slows conduction more when its axis is parallel to impulse propagation than when it is perpendicular”, which has been published in final form at [[DOI:10.1111/apha.13026](https://doi.org/10.1111/apha.13026)]. This article may be used for non-commercial purposes in accordance with Wiley Terms and Conditions for Self-Archiving.

<sup>1</sup> Department of Physiology, University of Bern, Bern, Switzerland

<sup>2</sup> Bertarelli Foundation Chair in Neuroprosthetic Technology, Laboratory for Soft Bioelectronic Interfaces, Institute of Microengineering, Institute of Bioengineering, Centre for Neuroprosthetics, École Polytechnique Fédérale de Lausanne (EPFL), Geneva, Switzerland

**Short title:** Cardiac conduction under uniaxial strain

**Keywords:** cardiac action potential; stretchable microelectrode arrays, cardiac cell cultures, stretch, strain, mechano-electrical feedback, conduction velocity, cable theory

Corresponding author (to whom proofs are to be sent):

Jan P. Kucera

Department of Physiology, University of Bern, Bühlplatz 5, CH-3012 Bern, Switzerland

Telephone: +41 31 631 87 59

Fax: +41 31 631 46 11

E-Mail: [kucera@pyl.unibe.ch](mailto:kucera@pyl.unibe.ch)

## Abstract

**Aim:** Cardiac tissue deformation can modify tissue resistance, membrane capacitance and ion currents, and hence cause arrhythmogenic slow conduction. Our aim was to investigate whether uniaxial strain causes different changes in conduction velocity ( $\theta$ ) when applied parallel vs. perpendicular to impulse propagation.

**Methods:** Cardiomyocyte strands were cultured on stretchable custom microelectrode arrays and  $\theta$  was determined during steady-state pacing. Uniaxial strain (5%), either parallel to (orthodromic) or perpendicular to (paradromic) propagation, was applied for 1 min and controlled by imaging a grid of markers. The results were analysed in terms of cable theory.

**Results:** Both types of strain induced immediate changes of  $\theta$  upon application and release. In material coordinates, orthodromic strain decreased  $\theta$  significantly more ( $p < 0.001$ ) than paradromic strain ( $2.2 \pm 0.5\%$  vs  $1.0 \pm 0.2\%$  in  $n=8$  mouse cardiomyocyte cultures,  $2.3 \pm 0.4\%$  vs  $0.9 \pm 0.5\%$  in  $n=4$  rat cardiomyocyte cultures, respectively). The larger effect of orthodromic strain can be explained by the increase of axial myoplasmic resistance, which is not altered by paradromic strain. Thus, changes in tissue resistance substantially contributed to the changes of  $\theta$  during strain, in addition to other influences (e.g., stretch-activated channels). Besides these immediate effects, the application of strain also consistently initiated a slow progressive decrease of  $\theta$  and a slow recovery of  $\theta$  upon release.

**Conclusion:** Potentially arrhythmogenic changes in cardiac conduction caused by acute stretch do not only depend on the magnitude of strain itself but also on the orientation of strain relative to impulse propagation. This dependence is due to different effects on tissue resistance.

**MeSH keywords:** Action Potentials; Biomechanical Phenomena; Electrophysiologic Techniques, Cardiac; Myocardium; Primary Cell Culture; Silicone Elastomers

## Introduction

During every cardiac cycle, the contraction of the cardiac chambers is triggered by a propagating action potential. The velocity of action potential propagation is a very important electrophysiological parameter. Conduction slowing is mechanistically involved in the generation and perpetuation of potentially life-threatening re-entrant arrhythmias (for a review, see <sup>1</sup>). Conduction velocity is determined by numerous factors, including the function of ion channels, the resistances of the myoplasm, the gap junctions and the extracellular space, the capacitance of the membrane, and the microscopic cellular architecture and content of the myocardium.<sup>1-4</sup>

While the mechanisms of normal and abnormal excitation and contraction have been extensively studied for more than a century,<sup>1,5,6</sup> the feedback of mechanical phenomena on the electrical function of the myocardium has comparatively received less attention. Mechano-electrical feedback is nevertheless an essential component of cardiac physiology and pathophysiology, because altered electrical function due to mechano-electrical feedback may have relevant repercussions on arrhythmogenesis.

Mechano-electrical feedback is mediated by a multitude of mechanisms. Experiments in isolated cells have shown that stretch of cardiomyocytes can modify the duration of the action potential, depolarize the resting membrane and induce triggered activity.<sup>7</sup> These effects are usually attributed to stretch-activated channels generating a depolarizing current.<sup>7-11</sup> Such channels can be constitutively present in cardiomyocytes, or be found in fibroblasts electrically coupled to myocytes.<sup>9,12,13</sup> Stretch may also modulate other ion channels, e.g., inwardly rectifying K<sup>+</sup> channels<sup>14</sup> and voltage-gated Na<sup>+</sup> channels,<sup>15</sup> which will affect the resting membrane potential and excitability.

Mechano-electrical feedback can also be mediated by changes in passive electrical properties.<sup>10,16</sup> Optical mapping experiments in volume-loaded Langendorff-perfused hearts

and anisotropically stretched cardiac cell cultures indicate that myocardial stretch alters the space constant of cardiac tissue and increases membrane capacitance via incorporation of caveolae into the cell membranes,<sup>17-19</sup> resulting in conduction slowing.

One aspect that has scarcely been investigated in experiments is whether conduction is affected differently if stretch occurs along the direction of propagation or transversely. Our hypothesis was that strain in the direction of propagation, which we term orthodromic strain, exerts a more pronounced effect than transverse strain (paradromic strain) due to an increase of tissue axial resistance, because orthodromic strain increases the dimension of cardiomyocytes along the path of propagation and decreases their cross-section. This hypothesis is relevant for arrhythmogenesis in the diseased heart because the relationship between the axes of strain and the direction of propagation may depend on the actual pathological condition leading to mechanical overload (e.g., ischemia, infarction, hypertrophy). Moreover, the spatiotemporal patterns of electrical activity and deformation may become mismatched during disorders characterized by large conduction delays and electro-mechanical dyssynchrony (e.g., bundle branch block).<sup>20</sup> A quantitative understanding of all the individual contributors to mechano-electrical feedback is also desirable to refine computational models of the contracting heart, which are expected to play an increasing role in personalized medicine.<sup>21-23</sup>

To address our hypothesis, we took advantage of a recently developed technology to fabricate stretchable silicone-based microelectrode arrays (sMEAs). The arrays consist of thermally evaporated thin gold electrodes and leads,<sup>24-26</sup> patterned and embedded in polydimethylsiloxane PDMS membranes, as illustrated in Fig. 1. The intrinsic microstructure of the gold film on PDMS (Fig. 1b) enables reversible deformation of the metallic film to tens of percent of applied strain.<sup>27</sup> Visual markers, also patterned within the gold film, allow for precise quantification of orthodromic and paradromic strains (see Methods). Patterned strands of cardiomyocytes were grown over rows of 6 recording electrodes and paced at their

extremity using stimulation dipole pairs (Fig. 2a-b). The sMEAs were interfaced with amplifiers and mounted in a setup consisting of four linear motorized stages enabling independent stretch along or perpendicular to the axis of the cell strands (Fig. 2c). Strain was monitored and adjusted in real time by imaging the markers (Fig. 2d). Using this *in vitro* electromechanical system, we monitored simultaneously the applied strain and action potential propagation. In parallel, we developed a mathematical framework based on cable theory to predict and interpret the effects of these two types of strain. According to this framework, the relative change of conduction velocity ( $\theta$ ) may be interpreted in terms of the different effects of strain on myoplasmic resistance and depends on the relative contribution of myoplasmic resistance to total axial resistance.

In the cultured strands, we show that conduction is slowed immediately upon the application of both types of strain, but the extent of this conduction slowing is larger for orthodromic strain than for paradromic strain, as predicted by our theoretical analysis. Furthermore, when the cell strands are held stretched at constant strain,  $\theta$  further decreases and does not recover entirely upon strain release. This indicates that besides immediate effects, sustained stretch also causes long-term phenomena that affect the electrical behaviour of cardiac tissue.

## Results

### Theoretical analysis of the effects of strain on conduction velocity

To permit an appropriate interpretation of the experimental results, it is essential to first conduct a theoretical analysis predicting the effects of uniaxial strain.  $\theta$  depends on membrane properties (ion currents and capacitance) and on the resistive properties of the tissue (gap junctions, myoplasm). Using material coordinates, we start by formulating the effects of stretch on  $\theta$  as

$$\theta(\lambda) = \bar{\theta} \cdot m(\lambda) \cdot q(\lambda) \quad (\text{Eq. 1})$$

with  $\lambda$  being the stretch factor ( $\lambda = 1 + \varepsilon$ ;  $\lambda=1$  for undeformed tissue) and  $\bar{\theta}$  being the reference  $\theta$  in undeformed tissue. The function  $m(\lambda)$ , with  $m(1)=1$ , represents the specific effect of stretch-induced changes of membrane properties (ion currents and capacitance) on  $\theta$ . Similarly, the function  $q(\lambda)$ , with  $q(1)=1$ , represents the specific effect of the changes in tissue resistance.

From cable theory, it is well known that  $\theta$  is related to axial tissue resistance ( $R$ , resistance in the direction of propagation) by an inverse square root law  $\theta \sim R^{-1/2}$ .<sup>2,28,29</sup> This inverse square root proportionality relationship is applicable when the space constant of the tissue and the spatial extent of the action potential upstroke are much larger than the size of a cell, such that the tissue can be considered homogeneous at a macroscopic scale. This is the case for rapid propagation in well coupled tissue, as in our experiments. The function  $q(\lambda)$  can therefore be formulated as

$$q(\lambda) = \left( \frac{R(\lambda)}{\bar{R}} \right)^{-1/2} \quad (\text{Eq. 2})$$

with  $\bar{R}$  being the axial resistance of the undeformed tissue ( $\bar{R} = R(1)$ ). The functions  $q(\lambda)$  and  $R(\lambda)$  also depend on the direction of strain (orthodromic vs. paradromic).

Because the cardiomyocyte cultures were seeded randomly on an isotropic substrate and formed strands that were considerably wider than cell size, the preparations were isotropic with no preferential orientation of the cells (Figure 2b). For isotropic tissue,  $m(\lambda)$  does not depend on the direction of uniaxial strain but only on the value of  $\lambda$ , in contrast to  $q(\lambda)$ . Tissue resistance is the sum of myoplasmic and junctional resistances, which are in series. Let

$\bar{R}_{\text{myo}}$  and  $\bar{R}_{\text{gap}}$  denote the corresponding resistances in undeformed tissue, with  $\bar{R} = \bar{R}_{\text{myo}} + \bar{R}_{\text{gap}}$ . To determine  $R(\lambda)$ , we consider now the dependence of myoplasmic and gap junctional resistance on  $\lambda$  for orthodromic strain ( $R_{\text{myo,ortho}}(\lambda)$  and  $R_{\text{gap,ortho}}(\lambda)$ ) and paradromic strain ( $R_{\text{myo,para}}(\lambda)$  and  $R_{\text{gap,para}}(\lambda)$ ).

During orthodromic strain, the tissue is elongated by a factor  $\lambda$  in the direction of propagation, whereas, assuming volume incompressibility, the cross section is decreased  $\lambda$ -fold (in the strict sense, in 3 dimensions, the tissue is compressed  $\lambda$ -fold in the  $z$ -direction). Because resistance is proportional to length and inversely proportional to cross-section,  $R_{\text{myo,ortho}}$  scales quadratically as  $R_{\text{myo,ortho}}(\lambda) = \bar{R}_{\text{myo}}\lambda^2$  (assuming that myoplasmic resistivity is not affected). In contrast, during paradromic strain, the cells are not elongated in the direction of propagation and the cross section does not change (incompressibility). Thus,  $R_{\text{myo,para}}(\lambda) = \bar{R}_{\text{myo}}$ .

The effects of stretch on gap junctional resistance can be formulated using another modulating function  $g(\lambda)$  as  $R_{\text{gap}}(\lambda) = g(\lambda) \cdot \bar{R}_{\text{gap}}$ , with  $g(1) = 1$ . Because of the same considerations as for  $m(\lambda)$  based on tissue isotropy,  $g(\lambda)$  depends only on  $\lambda$  but not on the direction of uniaxial strain. If the number and the biophysical properties of gap junctional channels do not change with strain, then  $g(\lambda)=1$ , because, in material coordinates, a given tissue region always consists of the same cells/channels upon deformation.

It is convenient to introduce  $f_{\text{myo}}$  and  $f_{\text{gap}}$  as constants describing the relative contribution of myoplasmic and gap junctional resistance to total resistance in the undeformed tissue as

$$\bar{R} = f_{\text{myo}} \cdot \bar{R} + f_{\text{gap}} \cdot \bar{R} = f_{\text{myo}} \cdot \bar{R} + (1 - f_{\text{myo}}) \cdot \bar{R}, \quad (\text{Eq. 3})$$

with  $f_{\text{myo}}+f_{\text{gap}}=1$ . For the two types of uniaxial strain, the following dependencies of  $R$  on  $\lambda$  can now be formulated as

$$R_{\text{ortho}}(\lambda) = f_{\text{myo}} \cdot \bar{R} \cdot \lambda^2 + (1 - f_{\text{myo}}) \cdot g(\lambda) \cdot \bar{R} \quad (\text{Eq. 4})$$

$$R_{\text{para}}(\lambda) = f_{\text{myo}} \cdot \bar{R} + (1 - f_{\text{myo}}) \cdot g(\lambda) \cdot \bar{R} \quad (\text{Eq. 5})$$

and, dividing by Eq. 3, taking the inverse square root and using Eq. 2, the functions  $q(\lambda)$  are

$$q_{\text{ortho}}(\lambda) = \left( \frac{R_{\text{ortho}}(\lambda)}{\bar{R}} \right)^{-1/2} = \left( f_{\text{myo}} \lambda^2 + (1 - f_{\text{myo}}) g(\lambda) \right)^{-1/2} \quad (\text{Eq. 6})$$

$$q_{\text{para}}(\lambda) = \left( \frac{R_{\text{para}}(\lambda)}{\bar{R}} \right)^{-1/2} = \left( f_{\text{myo}} + (1 - f_{\text{myo}}) g(\lambda) \right)^{-1/2}. \quad (\text{Eq. 7})$$

To evaluate how  $\theta$  varies with  $\lambda$  for small strains, we differentiate  $\theta(\lambda) = \bar{\theta} \cdot m(\lambda) \cdot q(\lambda)$  (Eq. 1) in respect to  $\lambda$  and evaluate the derivative at  $\lambda=1$ . For both types of uniaxial strain, we obtain

$$\frac{d\theta}{d\lambda} = \bar{\theta} \left( \frac{dm(\lambda)}{d\lambda} \cdot q(\lambda) + m(\lambda) \cdot \frac{dq(\lambda)}{d\lambda} \right),$$

and, at  $\lambda=1$ ,

$$\frac{d\theta}{d\lambda} \Big|_{\lambda=1} = \bar{\theta} \left( \frac{dm(\lambda)}{d\lambda} \Big|_{\lambda=1} + \frac{dq(\lambda)}{d\lambda} \Big|_{\lambda=1} \right), \text{ i.e.,}$$

$$\frac{d\theta/d\lambda|_{\lambda=1}}{\bar{\theta}} = \frac{dm(\lambda)}{d\lambda} \Big|_{\lambda=1} + \frac{dq(\lambda)}{d\lambda} \Big|_{\lambda=1}. \quad (\text{Eq. 8})$$

Let  $M = dm(\lambda)/d\lambda|_{\lambda=1}$  be the first summand on the right hand side. Although this term is not known a priori, it describes the specific effect of the changes in membrane properties on  $\theta$  near  $\lambda=1$ , which, due to isotropy, does not depend on the direction of uniaxial strain. This

contrasts with the second summand which differs for orthodromic and paradromic strain and is explicitly obtained from Eqs. 6 and 7 as

$$\frac{dq_{ortho}(\lambda)}{d\lambda} = -\frac{1}{2} \left( f_{myo} \lambda^2 + (1 - f_{myo}) g(\lambda) \right)^{-3/2} \left( 2f_{myo} \lambda + (1 - f_{myo}) \frac{dg(\lambda)}{d\lambda} \right) \quad (\text{Eq. 9})$$

$$\frac{dq_{para}(\lambda)}{d\lambda} = -\frac{1}{2} \left( f_{myo} + (1 - f_{myo}) g(\lambda) \right)^{-3/2} \left( (1 - f_{myo}) \frac{dg(\lambda)}{d\lambda} \right) \quad (\text{Eq. 10})$$

and, when evaluated at  $\lambda=1$ ,

$$\left. \frac{dq_{ortho}(\lambda)}{d\lambda} \right|_{\lambda=1} = -\frac{1}{2} \left( 2f_{myo} + (1 - f_{myo}) \left. \frac{dg(\lambda)}{d\lambda} \right|_{\lambda=1} \right) \quad (\text{Eq. 11})$$

$$\left. \frac{dq_{para}(\lambda)}{d\lambda} \right|_{\lambda=1} = -\frac{1}{2} \left( (1 - f_{myo}) \left. \frac{dg(\lambda)}{d\lambda} \right|_{\lambda=1} \right). \quad (\text{Eq. 12})$$

Let  $G = dg(\lambda)/d\lambda|_{\lambda=1}$ . Similarly to  $M$ ,  $G$  describes the specific effect of changes in gap junctional resistance on  $\theta$  near  $\lambda=1$ , which, due to isotropy, does not depend on the direction of uniaxial strain either. Substituting Eqs. 11 and 12 into Eq. 8 and using  $M = dm(\lambda)/d\lambda|_{\lambda=1}$  and  $f_{myo} + f_{gap} = 1$ , we finally obtain

$$\frac{d\theta_{ortho}/d\lambda|_{\lambda=1}}{\bar{\theta}} = M - \frac{1}{2} f_{gap} G - f_{myo} \quad (\text{Eq. 13})$$

and

$$\frac{d\theta_{para}/d\lambda|_{\lambda=1}}{\bar{\theta}} = M - \frac{1}{2} f_{gap} G. \quad (\text{Eq. 14})$$

Practically, we can apply these equations for small strains ( $\epsilon \ll 1$ ) as

$$\frac{(\theta_{\text{ortho}}(\epsilon) - \bar{\theta}) / \bar{\theta}}{\epsilon} = N_{\text{ortho}} = \left[ M - \frac{1}{2} f_{\text{gap}} G \right] - f_{\text{myo}} \quad (\text{Eq. 15})$$

and

$$\frac{(\theta_{\text{para}}(\epsilon) - \bar{\theta}) / \bar{\theta}}{\epsilon} = N_{\text{para}} = \left[ M - \frac{1}{2} f_{\text{gap}} G \right], \quad (\text{Eq. 16})$$

under the assumption that  $m(\lambda)$  and  $g(\lambda)$  are almost linear for  $\lambda$  between 1 and  $1+\epsilon$  such that  $M$  and  $G$  can be considered constant for small  $\epsilon$ . These equations describe the relative conduction velocity change normalized by strain, in the orthodromic ( $N_{\text{ortho}}$ ) and paradromic ( $N_{\text{para}}$ ) situations.

It can be noted that if both  $M$  and  $G$  are 0 (i.e., if strain does not affect membrane currents, capacitance or gap junctional resistance), paradromic strain exerts no effect on  $\theta$  ( $N_{\text{para}}=0$ ) while the effect of orthodromic strain is solely described by  $N_{\text{para}} = -f_{\text{myo}}$ . If  $G=0$  but  $M \neq 0$ , paradromic strain reflects solely the effects of changed membrane currents and/or capacitance ( $N_{\text{para}}=M$ ). Moreover, irrespective of  $M$  and  $G$ , the difference  $N_{\text{para}} - N_{\text{ortho}}$  is always  $f_{\text{myo}}$  and becomes small when  $f_{\text{myo}} \ll 1$ . Thus,  $N_{\text{para}} - N_{\text{ortho}}$  is only determined by  $f_{\text{myo}}$  and thus separates the effects of myoplasmic resistance on  $\theta$  from other effects.

Based on these considerations, we therefore analysed the experimentally measured effects of uniaxial strain on  $\theta$  by using material coordinates and by calculating  $N_{\text{ortho}}$  and  $N_{\text{para}}$  according to Eqs. 15 and 16, as well as the difference  $N_{\text{para}} - N_{\text{ortho}}$ .

It can nevertheless be noted that if true spatial (observer) coordinates are used to measure  $\theta$ ,  $N_{\text{ortho}}$  can be converted between both coordinate systems as

$$N_{\text{ortho,spatial}} = N_{\text{ortho,material}} + \frac{\theta_{\text{ortho,material}}}{\bar{\theta}} \approx N_{\text{ortho,material}} + 1 \quad (\text{Eq. 17})$$

while  $N_{\text{para}}$  is not changed. This means that during orthodromic strain, conduction can be slowed in material coordinates ( $N_{\text{ortho,material}} < 0$ ) but accelerated in observer coordinates ( $N_{\text{ortho,spatial}} > 0$ ), if  $-1 < N_{\text{ortho,material}} < 0$ .

### **In cultured cardiomyocyte strands, stretch and release induce an immediate and a progressive change of conduction velocity**

Figure 3a illustrates typical extracellular electrograms as recorded with each of the six recording microelectrodes on a beat-to-beat basis during continuous pacing in a strand of foetal murine cardiomyocytes in the undeformed state (left panel) and 4 seconds later (middle panel), immediately after the application of 10% orthodromic strain. Due to the high input impedance of the amplifiers, the strain and the subsequent increase of the resistance of the sMEA leads did not affect signal amplitude. As illustrated by the activation profiles (right panel), propagation was uniform at a  $\theta$  of 27.73 cm/s in the undeformed strand and 26.26 cm/s upon the application of 10% orthodromic strain, corresponding to a relative decrease by 5.3%. To evaluate the time-dependence of the effects of strain on  $\theta$ , cell strands were paced continuously, and 5% orthodromic strain was applied for predefined durations (Figure 3b). In the example shown in the left panel, the preparation was stretched 3 times for 10 s every 2 minutes. Stretch caused an immediate decrease of  $\theta$ , which, according to theory, can be attributed to the immediate increase of axial resistance. However, upon release,  $\theta$  recovered only slowly and incompletely to the baseline level. When the preparation was stretched for 1 min (middle panel), stretch and release caused similar immediate changes. However, interestingly,  $\theta$  progressively decreased during stretch and progressively (but incompletely) recovered after release. The right panel shows the behaviour of  $\theta$  in a preparation that was

stretched for 5 min.  $\theta$  was steadily decreasing, even at the end of the 5-min period. Recovery was slow and incomplete, even 5 min after release.

These immediate changes and slow trends of  $\theta$  were observed consistently in all experiments ( $n = 8$  foetal murine and 4 neonatal rat cardiomyocyte strands), indicating that stretch and release not only cause immediate acute changes of  $\theta$  that can be analysed in terms of the theory presented above, but also cause progressive electrophysiological changes over time scales of minutes. At such strain level ( $\leq 10\%$ ), the silicone mechanical behaviour is purely elastic and the observed slow drifts in  $\theta$  were therefore caused by biological adaptive mechanisms.

To be able to analyse the immediate effect of the two types of uniaxial strain as well as the long lasting progressive effect while minimizing the residual change of  $\theta$  resulting from long stretches, we next limited the periods of stretch to 1 min, and the preparation were pre-paced for 2 min before stretch.

### **The immediate change of conduction velocity upon stretch and release increases with strain amplitude and depends on the direction of strain**

Figure 3c illustrates the behaviour of  $\theta$  (in the material reference frame) in a cultured strand upon application and release of orthodromic and paradromic uniaxial strain of 5%, 8% and 10%. The immediate decrease of  $\theta$  upon stretch and its immediate increase upon release are visible at  $t=0$  and 60 sec, respectively. Because the linear stages were operating at a finite velocity of 3 mm/s, complete stretch and release were not instantaneous but took a few seconds (approx. 1.3 s for 5% and 2.5 s for 10% strain), corresponding, in this experiment, to 3-6 pacing cycles of 400 ms. The rapid change of  $\theta$  during mechanical deformation is illustrated in Fig. 3c insets. The timescale of the immediate changes of  $\theta$  (seconds) was considerably shorter than that of the progressive changes (minutes). Therefore, to quantify the

immediate effects of stretch and release, exponential fits (purple curves in Figure 3c) were applied to  $\theta$  before, during and after stretch and the change of  $\theta$  was measured from the difference between the exponential functions at the midpoints of stretch and release, respectively (green arrows). The change in  $\theta$  increased with the magnitude of strain, and was larger for orthodromic than for paradromic strain for all three magnitudes.

To analyse the measured changes of  $\theta$  in terms of the presented theoretical analysis, we examined the relative change of  $\theta$  vs. strain amplitude  $\varepsilon$ . Eqs. 15 and 16 predict that this relative change,  $(\theta_{\text{strain}}(\varepsilon) - \bar{\theta})/\bar{\theta}$ , is proportional to  $\varepsilon$ . Therefore, in Figure 4a, we represented  $\theta$  normalized by  $\bar{\theta}$  at stretch (left panels) and release (right panels) for orthodromic and paradromic strain (top and bottom panels, respectively). The normalization  $\theta$  was defined as  $\theta$  immediately before stretch and immediately after release, respectively. Figure 4a shows that the relative change of  $\theta$  increased in parallel with increasing strain magnitude and that it was larger for orthodromic than for paradromic strain. In Figure 4b, the relative changes of  $\theta$  were normalized by  $\varepsilon$  and represented vs.  $\varepsilon$ . In this experiment, the relative change of  $\theta$  was proportional to strain up to 10% without any manifest nonlinearity. The proportionality constants,  $N_{\text{ortho}}$  and  $N_{\text{para}}$  (Eqs. 15 and 16) were estimated by linear fits to the data. In this example, for stretch,  $N_{\text{ortho}}$  and  $N_{\text{para}}$  amounted to  $-0.52$  and  $-0.27$  and for release, to  $-0.40$  and  $-0.14$ , respectively. These negative values indicate that strain was associated with conduction slowing. Eqs. 15 and 16 predict that paradromic strain leads to a proportionality constant determined by changes of membrane properties and gap junctional coupling (parameters  $M$  and/or  $G$ ) whereas the proportionality constant for orthodromic strain also involves the term  $f_{\text{myo}}$ , the relative contribution of myoplasmic resistance to total axial resistance. Subtracting  $N_{\text{ortho}}$  from  $N_{\text{para}}$  for the experiment in Figure 4 gives a value of  $f_{\text{myo}}$  of  $0.25$  for stretch and a close value of  $0.27$  for release. This analysis indicates that during the one minute period during which strain was applied,  $M$  and/or  $G$  changed but  $f_{\text{myo}}$  did not.

Next, we analysed the change in conduction velocity in the spatial (Eulerian) reference frame (Fig. 4c). The comparison between material and spatial frames is important, because in the material frame,  $\theta$  is the velocity that is measured relative to the electrodes (which move with the preparation), while in the spatial frame  $\theta$  represents propagation velocity in the coordinate system of an outside observer, as it would be measured using optical mapping. Different experimental techniques are then linked to different frames. Fig. 4c shows that in the spatial reference frame, stretch paradoxically accelerated conduction along the direction of stretch while slowing it in the perpendicular direction.

### **Orthodromic vs. paradromic strain and the contribution of myoplasmic resistance**

In the next series of experiments, we stretched  $n=8$  strands of foetal mouse cardiomyocytes and  $n=4$  strands of neonatal rat cardiomyocytes to maximum 5% applied orthodromic and paradromic strain. Fig. 5a reports on the proportionality factors  $N_{ortho}$  and  $N_{para}$  for both species and types of applied uniaxial strain, for stretch and for release 1 min later. For both species and for both stretch and release, the effect of orthodromic strain was always 2-3 times larger than the effect of paradromic strain. For both mouse and rat cardiomyocyte cultures, this difference was statistically significant for both stretch and release ( $p<0.001$ , two-tailed paired Student's t-test). For both species, there was no difference in  $N_{ortho}$  and  $N_{para}$  between stretch and release. There was also no significant difference between preparations from mouse and rat cardiomyocytes.

Figure 5b shows the difference between  $N_{para}$  and  $N_{ortho}$  as an estimate of  $f_{myo}$ , the relative contribution of myoplasmic resistance to total axial resistance. There was no statistically significant difference between stretch and release and between species, and the averages values of  $f_{myo}$  were in the range 0.25-0.27. Based on our theory, these results suggest that the

myoplasm and gap junctions contribute about 1/4 and 3/4 to the axial resistance, respectively. These results also indicate that  $f_{nyo}$  is not changed after 1 min of stretch.

### **Stretch and release always initiate a slow progressive change of propagation velocity in addition to the immediate effect**

We observed that stretch typically initiated a progressive decrease of  $\theta$  whereas conduction progressively accelerated after release over a timescale of minutes (Figure 3, b and c). To assess how these decelerating/accelerating trends were superimposed on the immediate change of  $\theta$ , we examined the difference between the slopes of the exponential fits of  $\theta$  (examples in Figure 3c) at the time of stretch and release. This subtraction compensated for the fact that  $\theta$  had in some experiments not yet reached a perfect steady state before stretch, as it was still recovering from a previous one or still slowly accommodating to continuous pacing. These slope differences, normalized to reference  $\bar{\theta}$ , are reported in Figure 6 for all experiments with 5% orthodromic and paradromic strain applied for 1 min (same preparations as in Figure 5). At the onset of deformation, all values were negative irrespective of the type of strain and species, indicating that stretch initiated a progressive slowing of conduction in the range of a few percent per minute in all experiments. Conversely, at the time of release, all values were positive for both types of strain and both species. For both types of strain, the slope differences were significantly different from 0 ( $p < 0.05$ , two-tailed one-sample Student's t-test) in murine preparations at both the time of stretch and release, and in rat preparations at the time of stretch. This analysis confirms that in addition to immediate  $\theta$  changes, sustained stretch causes a slow progressive slowing of conduction, whereas release from sustained stretch causes a progressive recovery.

## Discussion

The effects of a deformation of cardiac tissue on its bioelectrical properties are multifaceted and complex. Understanding these effects and their different biophysical mechanisms requires a sound theoretical background and adequate experimental approaches in which predefined strains can be reliably applied and controlled while accurately monitoring impulse propagation. In this work we report on the successful use of stretchable microelectrode arrays to stimulate cardiac cell cultures and to record their electrical activity while accurately controlling the applied strain. Compared to alternative sMEA systems,<sup>24,30,31</sup> the precise control of the applied strain, independently controlled on the x and y axes, and its planar configuration are an asset. The combination of this technology with methods permitting to pattern the growth of cardiomyocyte cultures and thus to predetermine the direction of propagation provided an ideal setting that allowed us to address the question whether strain along the direction of propagation exerts a different effect from strain applied in the transverse direction.

We found that uniaxial strain of our cardiac cell cultures induces a two-stage effect on  $\theta$ : an immediate effect, which was larger for orthodromic than for paradromic strain and which can be interpreted in terms of the different effects of strain on myoplasmic resistance, and a slow effect that progressively increased during sustained strain and progressively dissipated after release.

### **The immediate effect of orthodromic vs. paradromic strain**

Axial tissue resistance is a primary determinant of  $\theta$ .<sup>2,28,29</sup> Therefore, it appears logical that strain in the direction of propagation and strain in the perpendicular direction should exert

different effects on conduction, since tissue resistance, notably myoplasmic resistance, directly depends on the shape of the deformed cells forming the tissue.

In material coordinates, under our experimental conditions, both orthodromic and paradromic strain caused conduction slowing that was proportional to strains up to 10%, a level that lies within the range reported during the cardiac contraction cycle.<sup>32</sup> However, the effect of orthodromic strain was about 2-3 times larger than that of paradromic strain. Thus, compared to paradromic strain, orthodromic strain caused an additional slowing. This significant additional slowing reveals the direction-dependent effect of strain on myoplasmic resistance. If axial resistance changed only negligibly during strain and exerted only minimal effects compared to other factors influencing conduction (e.g., rapidly responding stretch-activated currents, rapid changes of membrane capacitance, modulation of ion channel function), one would expect, due to the isotropy of the cultured strands, that  $\theta$  would change by the same amount during both orthodromic and paradromic strain. This was not the case in our experiments, indicating that myoplasmic resistance is a relevant contributor to changes of  $\theta$  during strain. Conversely, if changes of  $\theta$  were exclusively due to changes in myoplasmic resistance, then paradromic strain would be expected not to change  $\theta$ . This was also not the case in our experiments, indicating that other factors were also involved in the observed changes of  $\theta$ .

As formalized by Eqs. 15 and 16, paradromic strain reveals effects that are not accounted by changes in myoplasmic resistance, while orthodromic strain reveals, in addition, the specific effects of myoplasmic resistance. In our experimental setting, our results suggest that during orthodromic strain, about 50-65% of the decrease of  $\theta$  was due to an increase of myoplasmic resistance, while 35-50% was due to other effects. Thus, the contribution of changes in myoplasmic resistance was as important as that of other mechano-electrical feedback mechanisms. While we did not investigate these other mechanisms in specific experiments, a

likely candidate is the activation of stretch-activated channels, causing resting membrane depolarization and thus partial inactivation of  $\text{Na}^+$  channels.<sup>13</sup>

According to theory, from the difference between the proportionality constants relating strain to the normalized change of  $\theta$ , it is possible to estimate  $f_{\text{myo}}$ , the relative contribution of myoplasmic resistance to total axial resistance. In our experiments, we found values in the range of 25% for cultures of both mouse and rat ventricular myocytes. In intact myocardium, the different components of axial resistance are typically quantified using impedance spectrometry.<sup>28,33</sup> Based on the data of Dhillon *et al.*,<sup>28</sup>  $f_{\text{myo}}$  is approximately 25% in the left ventricle, 43% in the left atrium and 50% in the right atrium of the guinea pig. Our estimated value lies in the same range, although a direct comparison is not possible because the previously published measurements were done in the intact myocardium of a different species. However, our estimation is somewhat inferior to what is assumed based on combined experimental and computer simulation studies (about 50%<sup>34-36</sup>). Nevertheless, our study suggests that precise measurements of  $\theta$  in different directions combined with accurate measurements of strain may represent an adequate tool to quantify the individual components of tissue axial resistance, and how these components are altered under pathological conditions. For example, under conditions of reduced gap junctional coupling encountered e.g., during heart failure or upon ischemia,<sup>37</sup> it is expected that the difference between the response of  $\theta$  to orthodromic vs. paradromic strain will be smaller, because  $f_{\text{myo}}$  will be closer to 0.

It must be mentioned that in intact myocardium,  $f_{\text{myo}}$  would also account for the relative contribution of the resistance of the extracellular space to total axial resistance, which is expected to scale similarly with strain as myoplasmic resistance (Eqs. 4 and 5). Thus, by generalization,  $f_{\text{myo}}$  represents the ratio of non-junctional to total tissue resistance.

In intact myocardium, an additional level of complexity will arise due to the anisotropy of its conductive properties. These properties can mathematically be described by a conductivity

tensor with three principal axes, one oriented along the fibre direction, the second perpendicular to it but oriented along sheets of myocytes, and the third oriented normal to the myocyte sheets.<sup>38</sup> The effect of strain will thus depend on the relative three-dimensional orientation of the principal axes of this conductivity tensor, of the principal axes of the stretch tensor, and of the vector characterizing action potential propagation. Our theory is based on a linearization of the behaviour of  $\theta$  near the reference undeformed state. It can, if needed, be extended to account for arbitrary conductivity tensors, deformations, and directions of propagation using appropriate tensor calculus.<sup>10,38</sup> It must also be mentioned that in three dimensions, true uniaxial strain of the myocardium cannot be obtained because cells are incompressible. The product of the three principal stretches (eigenvalues  $\lambda$  of the stretch tensor) must always equal 1. This was taken into account in our theory by considering that the preparation is stretched by a factor  $1/\lambda$  (i.e., compressed by a factor  $\lambda$ ) in the direction normal to the cell culture. Hence, myoplasmic resistance is unchanged if length is increased  $\lambda$ -fold while cross-section is decreased  $\lambda$ -fold. Thus, our mathematical framework remains valid by extending the notion of orthodromic strain to the situation in which the direction of propagation coincides with the stretch axis associated to the largest  $\lambda$ , and by extending the notion of paradromic strain to the situation where the direction of propagation coincides with a stretch axis associated with an eigenvalue  $\lambda=1$ . Our framework can therefore be generalized and applied, e.g., to analyse and interpret the data obtained using new experimental techniques permitting the simultaneous optical mapping of both excitation and deformation of the whole heart.<sup>39</sup>

The relationship between strain and  $\theta$  has been previously examined in a number of experimental studies, as reviewed by McNary *et al.*<sup>10</sup> Some studies report that conduction is accelerated upon strain, some report conduction slowing, while further studies report an initial increase of  $\theta$  followed by a decrease at larger strains. These discrepancies may be due to the different preparations used, the different experimental conditions and the different levels of

strain. These differences may lead to variable contributions of the factors modulating  $\theta$ . However, it is important to realize that the behaviour of  $\theta$  depends on the coordinate system chosen to quantify  $\theta$  (material vs. spatial coordinates). This choice is often inherent to the experimental technique used and depends on the settings of a particular study. Our results show that conduction can be slowed in material coordinates, while accelerated in spatial coordinates. Our findings are in agreement with those of Grand *et al.*,<sup>13</sup> who assessed  $\theta$  using optical mapping of cardiomyocyte strands during orthodromic (but not uniaxial) strain and showed that depending on the coordinates used, conduction can appear to be either slowed or accelerated.

### **The progressive effect of strain on conduction**

In addition to the rapid response of  $\theta$  to stretch and release, we consistently observed that on a time scale of minutes,  $\theta$  progressively decreases during sustained stretch and progressively recovers upon release. By permitting long-term measurements on a beat-to-beat basis, the use of stretchable microelectrode arrays was crucial in revealing these progressive changes. Such long-term measurements are not possible using optical mapping with voltage-sensitive fluorescent dyes because the latter induce cumulative photodynamic damage to the preparations. The presence of these slow drifts of  $\theta$  indicates that it is desirable to control and report the duration of the applied deformation in any experiments aiming at the study of the strain-velocity relationship.

Over several minutes, the slow decrease of  $\theta$  during strain can become substantial and reach a similar magnitude as that of the immediate effect (Figure 3b). In an optical mapping study, Pfeiffer *et al.*<sup>19</sup> investigated the change of  $\theta$  consecutive to 1 min. of pressure overload in Langendorff-perfused murine hearts and 5 min. of anisotropic biaxial strain (14%/3.6%) in murine ventricular cell cultures. In the latter, they observed a decrease of  $\theta$  by 26% in spatial

coordinates, translating to approx. 40% decrease in material coordinates, which is considerably larger than what we observed. This difference can be explained by the larger strain used (14% vs. 5% in our study) and by the combination of both orthodromic and paradromic strain, which would exert additive effects. Also, after a period of 5 min., it is possible that the large decrease of  $\theta$  resulted from the summation of the immediate and progressive effects of strain. Importantly, Pfeiffer et al. also showed that the decrease of  $\theta$  is blunted in caveolin-3 knockout murine preparations and that in wild-type myocardium, stretch causes a fusion of caveolae with the plasma membrane that increases membrane capacitance. These results indicate an important long-term role of membrane capacitance in mechano-electrical feedback. The incorporation of caveolae into the membrane is an active biological process that certainly occurs over time scales that are longer than the biophysical effect of strain on tissue resistance and ion channel gating. It is therefore quite plausible that the slow changes of  $\theta$  that we observed were due to changes of membrane capacitance due to caveolae trafficking.

It is known that long periods of myocardial stretch cause a profound remodelling of morphological and electrophysiological properties.<sup>40-43</sup> In cardiomyocyte cultures, Zhuang et al.<sup>40</sup> showed that the expression of connexin 43 and  $\theta$  are increased after 1 hour of static stretch. In contrast, in the canine ventricle in vivo, Hussain et al.<sup>43</sup> showed that 6 hours of sustained stretch decreases transverse  $\theta$  and remodels the distribution of gap junctions. A progressive increase of gap junctional coupling as reported by Zhuang et al. is unlikely to have contributed to the slow changes of  $\theta$  that we observed, because our experiments were executed over a much shorter period and because an increase of gap junctional coupling would, in fact, have accelerated conduction and increased  $f_{\text{myo}}$  at release, which we did not observe.

To elucidate all possible mechano-electrical feedback mechanisms in detail during orthodromic and paradromic strain would require dedicated experiments, e.g., with blockers

of stretch-activated channels, agents that interfere with the recruitment of caveolae, or modulators of gap junctions. These experiments were beyond the scope of our work.

### **Implications for arrhythmogenesis in clinical settings**

Slow conduction, in conjunction with conduction block and triggered activity, is mechanistically involved in the generation of re-entrant arrhythmias.<sup>1</sup> Conduction velocity reflects the capacity of depolarized tissue at the wavefront to activate resting tissue downstream. Any intervention that decreases tissue resistance will therefore impact on this capacity. Our results indicate that tissue resistance is an important component that modulates conduction during stretch.

The relative changes of  $\theta$  that we report are in the range of a few percent and thus, in the healthy heart with a homogeneous tissue structure, these changes are unlikely to play any major arrhythmogenic role. However, the situation is different in the diseased heart, in which tissue structure becomes heterogeneous, e.g., at the periphery of infarct scars or in cardiac fibrosis consecutive to ischemia, hypertrophy and ageing. Such tissue is characterized by a discontinuous substrate<sup>44-46</sup> with tissue expansions and branching giving rise to irregular conduction patterns. Under these conditions, the effect of variations of tissue resistance on  $\theta$  will be amplified and these variations may modulate the propensity to conduction block. In computer simulations, Fast and Kléber<sup>47</sup> have shown that at tissue expansions, the propensity to conduction block is decreased if tissue resistance is increased in the axis of the expansion but unchanged when transverse tissue resistance is increased. Thus, in diseased cardiac muscle, orthodromic vs. paradromic strain may not only exert different effects on  $\theta$  but also affect the risk of block in different manners. Thus, these two forms of strain may have different arrhythmogenic consequences.

It is however not straightforward to anticipate to which type of strain (or combination thereof) distinct regions of the beating heart will be subjected during acute overload. Due to their cylindrical anatomical structure, Purkinje fibres and papillary muscles will typically undergo orthodromic strain. Paradromic strain could be encountered, e.g., when a region with delayed activation (e.g., in an infarct scar) is stretched from the side by an already contracting region that was activated earlier. During fibrillation, re-entrant spiral waves continuously change direction and re-excite the myocardium, which results in complex spatiotemporal patterns of heterogeneous strain determining the onset and dynamics of the arrhythmia.<sup>48,49</sup> During fibrillation, a patchwork of orthodromic vs. paradromic strain is expected to occur, and their different effects may further influence the stability and the perpetuation of the arrhythmia.

It is expected that multiphysics bioelectrical-biomechanical computer models of the contracting heart tailored to individual patients will play an important role in personalized medicine.<sup>21-23</sup> Based on our findings, we advocate that modern models should always incorporate the effect of deformation on tissue resistance. This represents an additional computational burden, since electrical conductivities between discrete model nodes must continuously be recomputed, but omitting to do so may result in less accurate model predictions.

## **Conclusion**

We have developed a unique experimental system to accurately measure the changes in cardiac conduction induced by controlled strain. Our findings are important for a comprehensive understanding of mechano-electrical feedback and of arrhythmias in general. It is hoped that further developments in materials science will lead to the development of even more versatile devices, which would definitely permit to obtain deeper insights into the interaction between bioelectrical and biomechanical phenomena *in vitro* and *in vivo*.

## Materials and methods

### Ethical approval

Animals were handled in accordance with the ethical principles and guidelines of the Swiss Academy of Medical Sciences. The procurement of animals, the husbandry and the experiments conformed to the European Convention for the Protection of Vertebrate Animals used for Experimental and other Scientific Purposes. The protocols were reviewed and authorized by the Commission of Animal Experimentation of the Cantonal Veterinary Office of the Canton of Bern, Switzerland.

### Design and fabrication of stretchable microelectrode arrays (sMEAs)

Four-inch silicon wafers were first activated by oxygen plasma and spin-coated (1500 rpm for 1 min) with a water-soluble layer of poly(4-styrenesulfonic acid) (PSS; 18 wt. % in H<sub>2</sub>O; Sigma-Aldrich, Buchs, Switzerland), which was dried on a hot plate for 5 min at 160 °C. Then, a ~0.5 mm thick polydimethylsiloxane layer (PDMS, Sylgard<sup>®</sup> 184, 10/1 (wt/wt) base/curing agent, Dow Corning) was spin-coated on the wafers (100 rpm for 1 min) and cured for  $\geq 2$  h at 75-80 °C. Subsequently, a 5 nm thick layer of chromium and a 45 nm thick layer of gold were successively thermally evaporated on the PDMS surface through a 50  $\mu$ m thick polyimide stencil mask (Laser Micromachining Ltd, St. Asaph, UK). The mask also incorporated markers (discs of 100  $\mu$ m diameter) arranged in a square lattice arranged in a square lattice (Fig. 1a) to quantify the effective applied strain (see below). The thin gold film on PDMS is characterized by interconnected regions separated by microscopic cracks and clefts (Figure 1b). As shown previously,<sup>27</sup> due to the widening of these clefts without overall

rupture of the metallic layer, the film remained conductive when stretched by up to 20% uniaxial strain. The resistance of the leads was in the k $\Omega$  range and increased 2-4 fold upon a uniaxial stretch of 20%, in agreement with previous observations.<sup>27</sup>

The array interconnects were encapsulated with a 10-15  $\mu\text{m}$  thick PDMS layer in the 2x2 cm central region of the array.<sup>25</sup> To process the encapsulation layer, diluted PSS (9 wt. % in deionised H<sub>2</sub>O) was spin-coated (1500 rpm for 1min) on 1-2 mm thick layer of PDMS after oxygen plasma surface activation. The water soluble release layer was dried at room temperature for 1 hour. The PDMS encapsulation layer was then spin-coated (5000 rpm for 1 min) and cured. Electrode contacts (330 or 1450  $\mu\text{m}$  in diameter) were first opened by perforation through the thin PDMS layer. The perforated encapsulation layer was then aligned and bonded on the microelectrode array after activation with oxygen plasma. Next, the encapsulated sMEA was immersed in deionised water at 36 °C, which led to the spontaneous release of the array from the silicon carrier wafer after a few hours.

To allow for independent stretch in perpendicular directions, the sMEAs were designed with a biaxial symmetric shape (Figure 1a and 1c). Holes (3 mm diameter) were punched at sites corresponding to screws holding printed circuit boards interfacing the sMEA electrically and mechanically with the stretching system (Figure 1c). The smooth curved shape of the sMEA edge between the connecting pads was designed to minimize strain heterogeneity in the sMEA centre,<sup>50</sup> to prevent excessive stretching of the gold leads in the off-centre region, and to account for the propensity of the PDMS layer to tear at sharp concave angles.

The sMEAs incorporated 2 rows of 6 recording electrodes spaced 1 mm from each other. These electrodes consisted of the rounded tip of the gold leads (diameter 200  $\mu\text{m}$ ) exposed through the 330  $\mu\text{m}$  diameter holes perforated in the encapsulation layer. At both ends of each row, stimulation dipoles were patterned as pairs of 1.6 mm half-discs (exposed through the 1450  $\mu\text{m}$  holes). Contact pads for the recording microelectrodes and stimulation dipoles were distributed along four edges of the array.

To form a culture chamber, a hollow PDMS cylinder (inner diameter: 17.5 mm; outer diameter: 22 mm; height: 15 mm) was affixed using Vaseline on the centre of the sMEA. During stretch, the Vaseline permitted the cylinder to slide freely on the sMEA without interfering with its deformation while preventing any leak of medium. The sliding did not affect the resistance of the sMEA leads.

### **Patterned cardiac cell cultures on sMEAs**

Foetal murine cardiomyocyte cultures were prepared according to previously published procedures.<sup>51-53</sup> Briefly, ventricles of wild-type C57BL6/J mice were obtained from fetuses at postcoital day 19, minced, and digested enzymatically. After preplating for 2 h to minimize myofibroblast content, the cells were seeded at a density of  $3.5 \cdot 10^5/\text{cm}^2$  on the sMEAs sterilized with ultraviolet light. Cultures of neonatal rat ventricular myocytes were prepared in a similar manner from the ventricles of 1 day old Wistar rats, as previously described,<sup>54</sup> and seeded at a density of  $2 \cdot 10^5/\text{cm}^2$ . Unless specified otherwise, data are presented for foetal murine cardiomyocyte cultures.

Tissue patterns with a predefined geometry corresponding to the sMEA electrode layout (Figure 2a and 2b) were prepared using a lift-off technique. First, a laser-machined 50  $\mu\text{m}$  thick polyimide mask was aligned and placed on the sMEA. The sMEA was then preconditioned with type I collagen (Sigma-Aldrich Buchs, Switzerland) to permit the attachment of the cells on the exposed and sterilized surface of the sMEA. One day after seeding, the mask and the cells that had attached on top of it were then removed, leaving the designed tissue pattern (Figure 2a and 2b). The pattern consisted of 2 strands (width: 600  $\mu\text{m}$ ; length: 0.9 cm) passing over the 2 rows of 6 extracellular electrodes. At each strand extremity, the strands merged into wider disc-shaped structures covering the corresponding stimulation dipoles. This pattern thus channelled impulse propagation along the direction of the strands.

The cultures were incubated with M199 medium with Hanks' salts (Sigma-Aldrich, Buchs, Switzerland) supplemented with streptomycin (20 mg/L, Oxoid, Pratteln, Switzerland) and penicillin (20000 U/L, Oxoid, Pratteln, Switzerland). Bromodeoxyuridine (100  $\mu\text{mol/L}$ , Sigma-Aldrich, Buchs, Switzerland) was also added to inhibit myofibroblast proliferation.

### **Stretching system, imaging, measurement and control of strain**

The sMEAs were mounted on a custom-made stretching system consisting of 4 linear motorized stages (MTS25-Z8, Thorlabs, Newton, New Jersey) arranged in a symmetric manner on which printed circuit boards (PCB) destined to hold the sMEA were tightly fixed (Figure 2c). Each sMEA edge was clamped onto one of these PCBs using a second PCB incorporating connecting pads, aligned on the sMEA and held using two screws (Figure 2c, inset). The edges of the PCBs were filed to avoid damage to the sMEA leads. To avoid any sliding at the sMEA-PCB interface, the bottom PCB was covered with sandpaper. To optimize electrical contact between the sMEA and the PCB leads, a small amount of conductive paste (EPO-TEK H27D, Epoxy Technology, Billerica, MA, USA) was applied on the connecting pads. Using the motorized stages, the sMEA was centred on the system in a reference unstretched configuration.

To deform the sMEA with principal strains oriented along the axes of the system, opposite linear stages were operated identically and synchronously. To measure and monitor strain, the sMEA were illuminated from above using a LED array and imaged from below using a digital camera (B910 HD Webcam, Logitech, Lausanne, Switzerland) operating in the zoom mode at 640x480 pixels. This approach permitted to image the fiducial markers on the sMEA without any distortion due to refraction at the air-medium interface. To compensate the lens distortion of the camera, a fixed grid of points (1 mm pitch) was first imaged and used as calibration in a warping procedure which was applied to all subsequent images. Strain was quantified by

analysing an image of the deformed sMEA relative to the reference image of the undeformed sMEA. The centroid coordinates (in pixels) of the fiducial markers were identified using a custom program written in MATLAB (The MathWorks, Natick, MA, USA), and the following affine map was then fitted on the two sets of coordinates:

$$\begin{pmatrix} x_i \\ y_i \end{pmatrix} = \begin{pmatrix} t_x \\ t_y \end{pmatrix} + \begin{pmatrix} F_{xx} & F_{xy} \\ F_{yx} & F_{yy} \end{pmatrix} \begin{pmatrix} X_i \\ Y_i \end{pmatrix}, \quad (\text{Eq. 18})$$

where  $(X_i, Y_i)$  and  $(x_i, y_i)$  are the coordinates of the  $i^{\text{th}}$  marker in the reference and deformed configuration, respectively,  $(t_x, t_y)$  is a translation vector dependent on the arbitrary choice of the origin, and the matrix given by  $F_{xx}$ ,  $F_{xy}$ ,  $F_{yx}$  and  $F_{yy}$  represents the deformation gradient tensor  $F$ . A polar decomposition was then performed on  $F$  as  $F=RU$ , where  $R$  is a rotation matrix and  $U$  is the symmetric right stretch tensor. The rotation component was usually  $<2$  degrees. Principal strains and confidence intervals, as well as and their orthogonal directions were then obtained from the eigenvalues ( $\lambda_x$  and  $\lambda_y$ ) and the corresponding eigenvectors of  $U$ . The deviation of the stretch directions from the axes of the sMEA (the x-axis being defined by the cultured strands) was negligible ( $< 1$  degree). The corresponding strains were then determined as  $\varepsilon_x=1-\lambda_x$  and  $\varepsilon_y=1-\lambda_y$  (engineering strain) and expressed in percent. Using this approach,  $\varepsilon_x$  and  $\varepsilon_y$  could be determined with an absolute precision (95% confidence interval) in the range of 0.2%.

The linear affine map used above presupposes that the deformation and thus  $F$  is homogeneous over the entire region delimited by the markers. To ascertain whether the deformation was heterogeneous,  $x_i$  and  $y_i$  were also fitted with quadratic functions of  $X_i$  and  $Y_i$ , and Akaike's information criterion was used to identify the fitting model with the highest likelihood.<sup>55</sup> In the vast majority of experiments ( $>99\%$ ), no additional information was gained using the quadratic fit while the root mean square residual error (typically  $\sim 0.25$

pixels) did not decrease significantly, indicating that within measurement error, the strain was homogeneous in the central part of the sMEAs.

Due to the Poisson effect, stretching the sMEA along a given axis resulted in stricture in the perpendicular direction in the centre of the sMEA. Therefore, to obtain uniaxial strain in the direction of impulse propagation (orthodromic strain) or perpendicular to it (paradromic strain), the Poisson effect was compensated by stretching the sMEA using the second pair of linear stages. In each experiment, the strain applied by the two pairs of stages was adjusted iteratively in real time using a custom program until the target values of  $\epsilon_x$  and  $\epsilon_y$  were reached within their 95% confidence interval (Figure 2d), and the stage positions were saved. The viscosity of the Vaseline seal did not induce any delay in applying the strain, which was stable  $<0.2$  s after cessation of stage motion. The stages were operated at their maximal velocity (3 mm/s) and the different strains could be recalled and reliably applied in 1-3 s.

### **Electrophysiological experiments**

Using the interfacing PCBs, the sMEAs were connected to a previously described custom stimulation and recording system.<sup>56</sup> Prior to the experiments, the culture medium was replaced with Hanks' balanced salt solution (Sigma-Aldrich). Using the stimulation dipoles, the cultured strands were paced at one extremity using biphasic voltage pulses at 1.5-2x diastolic threshold (0.8-2 V, 1-2 ms duration) at a cycle length of 300-1000 ms, which was adjusted to be short enough to overdrive any spontaneous activity but long enough to minimize any effects of action potential restitution behaviour. As ground electrode, a 0.3 mm thick gold wire, forge-hammered to increase its surface and bent into a loop was immersed into the medium (Figure 2c and 2d). Unipolar extracellular electrograms from the recording electrodes were amplified (gain: 1000x; bandwidth: 0.1-3 kHz), digitized (12 bit) and sampled at 10 kHz. The entire system was enclosed in a polystyrene box covered with aluminium foil

and warmed to 37 °C with humidified air using a precision heater (The Cube, Life Imaging Services, Basel, Switzerland). The temperature probe was positioned in the immediate vicinity of the culture chamber. Target temperature was reached in ~20 min and experiments were started after an additional 20 min equilibration period.

After  $\geq 2$  min of continuous pacing permitting conduction to accommodate, 5% orthodromic uniaxial strain ( $\epsilon_x=0.05$  and  $\epsilon_y=0$ ) was applied and maintained for a predefined duration, after which the sMEA was released to its undeformed state while pacing was continued for  $\geq 1$  min. The same procedure was then repeated with 5% paradromic strain ( $\epsilon_x=0$  and  $\epsilon_y=0.05$ ). This protocol was then repeated for larger uniaxial strains (8% and 10%). However, at these strain levels, the integrity of some recording leads was often lost. If  $>3$  channels were lost, these measurements were disregarded since the accurate determination of conduction velocity was precluded. Thus, only a subset of preparations was subjected to strains of 8% and/or 10%. To permit the unbiased analysis of the time course of conduction velocity ( $\theta$ ) before, during and after a given strain, the same subset of electrodes was used to determine  $\theta$ .

### **Determination of conduction velocity**

Classically,  $\theta$  is determined by identifying the activation time (AT) at each electrode (typically, the occurrence of the minimum of the electrogram derivative), by performing a linear regression of AT vs. distance  $x$ , and by obtaining  $\theta$  as the inverse of the slope.<sup>56</sup> This approach however suffers from inaccuracies in the determination of ATs and from their round-off to the next integer multiple of the sampling period (if the signals are not interpolated). As a more reliable method, we computed, as previously described,<sup>57,58</sup> the conduction delays between all possible pairs of electrodes by finding the interpolated time of the negative-to-positive zero crossing of the Hilbert transform of the autocorrelation function of the corresponding signals. A linear function of time  $a(x)=x/\theta+k$  was then fit to minimize

the sum of the squared differences between the measured and fitted conduction delays. We note that this approach does not permit to compute the ATs directly, since the equation system is undetermined for  $k$ . However,  $k$  is a constant time offset determined only by the arbitrary choice of the reference time  $t=0$  and is not needed for the calculation of  $\theta$ .

We used the reference positions of the electrodes in the undeformed sMEA to calculate  $\theta$ . Thus,  $\theta$  was determined in material (Lagrangian) coordinates ( $\theta_{\text{mat}}$ ), since the cells attached to a given electrode move jointly with it. This differs from experiments in which  $\theta$  is determined using optical mapping with a rigid light-sensing device,<sup>13,19</sup> in which individual photodetectors register the fluorescence of a different group of cells upon stretch. In the latter approach,  $\theta$  is represented in the spatial (Eulerian) coordinates of the observer ( $\theta_{\text{obs}}$ ). Unless specified otherwise,  $\theta$  is given in material coordinates. However, because the strain was uniaxial with its axis parallel/perpendicular to the row of electrodes and the direction of propagation,  $\theta_{\text{obs}}$  can be obtained from  $\theta_{\text{mat}}$  as  $\theta_{\text{obs}} = (1+\epsilon)\cdot\theta_{\text{mat}}$  for orthodromic strain and  $\theta_{\text{obs}} = \theta_{\text{mat}}$  for paradromic strain.

## Statistics

All analyses and computations were conducted using MATLAB. Significance was assessed using the two-tailed Student's t-test (paired, one-sample or two-sample as appropriate).

## Acknowledgments

We are greatly indebted to Helene Hinnen and Regula Flückiger Labrada for the preparation of the cultures, Dr. h. c. Denis de Limoges and Christian Dellenbach for their support with the electronics of the setup as well as Aaron Gerratt, Sandra Gribi and Anthony Guillet for their advice and technical support with the sMEA fabrication.

## **Conflict of interest**

The authors have no competing interests to disclose.

## **Funding**

This work was supported by the Swiss National Science Foundation (grant number 31003A\_156738 to J.P.K. and grant number BSCGIO\_157800 to S.P.L.) and by the Bertarelli Foundation.

## References

1. Kléber, AG, Rudy, Y: Basic mechanisms of cardiac impulse propagation and associated arrhythmias. *Physiol Rev*, **84**: 431-488, 2004.
2. King, JH, Huang, CL, Fraser, JA: Determinants of myocardial conduction velocity: implications for arrhythmogenesis. *Front Physiol*, **4**: 154, 2013.
3. Spach, M, Dolber, P, Heidlage, J: Properties of discontinuous anisotropic propagation at a microscopic level. *Ann NY Acad Sci*, **591**: 62-74, 1990.
4. Kohl, P, Camelliti, P, Burton, FL, Smith, GL: Electrical coupling of fibroblasts and myocytes: relevance for cardiac propagation. *J Electrocardiol*, **38**: 45-50, 2005.
5. Katz, AM: Ernest Henry Starling, his predecessors, and the "Law of the Heart". *Circulation*, **106**: 2986-2992, 2002.
6. Bers, DM: Cardiac excitation-contraction coupling. *Nature*, **415**: 198-205, 2002.
7. Riemer, TL, Tung, L: Stretch-induced excitation and action potential changes of single cardiac cells. *Prog Biophys Mol Biol*, **82**: 97-110, 2003.
8. Kohl, P, Bollensdorff, C, Garny, A: Effects of mechanosensitive ion channels on ventricular electrophysiology: experimental and theoretical models. *Exp Physiol*, **91**: 307-321, 2006.
9. Kohl, P, Kamkin, AG, Kiseleva, IS, Noble, D: Mechanosensitive fibroblasts in the sinoatrial node region of rat heart: interaction with cardiomyocytes and possible role. *Exp Physiol*, **79**: 943-956, 1994.
10. McNary, TG, Sohn, K, Taccardi, B, Sachse, FB: Experimental and computational studies of strain-conduction velocity relationships in cardiac tissue. *Prog Biophys Mol Biol*, **97**: 383-400, 2008.
11. Kamkin, A, Kiseleva, I, Wagner, KD, Scholz, H: Mechano-electric feedback in the heart: Evidence from intracellular microelectrode recordings on multicellular preparations and

- single cells from healthy and diseased tissue. In: *Mechanosensitivity in Cells and Tissues*. edited by Kamkin, A., Kiseleva, I., Moscow, 2005.
12. Quinn, TA, Camelliti, P, Rog-Zielinska, EA, Siedlecka, U, Poggioli, T, O'Toole, ET, Knopfel, T, Kohl, P: Electrotonic coupling of excitable and nonexcitable cells in the heart revealed by optogenetics. *Proc Natl Acad Sci U S A*, **113**: 14852-14857, 2016.
  13. Grand, T, Salvarani, N, Jousset, F, Rohr, S: Aggravation of cardiac myofibroblast arrhythmogenicity by mechanical stress. *Cardiovasc Res*, **104**: 489-500, 2014.
  14. McNary, TG, Sachse, FB: Modeling effects of strain-modulated membrane capacitance and conductance of K<sup>+</sup> inward rectifier on conduction velocity in cardiac tissue. *IEEE Comp Cardiol*, **36**: 381-384, 2009.
  15. Beyder, A, Rae, JL, Bernard, C, Strege, PR, Sachs, F, Farrugia, G: Mechanosensitivity of Na<sub>v</sub>1.5, a voltage-sensitive sodium channel. *J Physiol*, **588**: 4969-4985, 2010.
  16. Sachse, FB, Steadman, BW, JH, BB, Punske, BB, Taccardi, B: Conduction velocity in myocardium modulated by strain: measurement instrumentation and initial results. *Conf Proc IEEE Eng Med Biol Soc*, **5**: 3593-3596, 2004.
  17. Mills, RW, Narayan, SM, McCulloch, AD: Mechanisms of conduction slowing during myocardial stretch by ventricular volume loading in the rabbit. *Am J Physiol Heart Circ Physiol*, **295**: H1270-H1278, 2008.
  18. Zhang, Y, Sekar, RB, McCulloch, AD, Tung, L: Cell cultures as models of cardiac mechanoelectric feedback. *Prog Biophys Mol Biol*, **97**: 367-382, 2008.
  19. Pfeiffer, ER, Wright, AT, Edwards, AG, Stowe, JC, McNall, K, Tan, J, Niesman, I, Patel, HH, Roth, DM, Omens, JH, McCulloch, AD: Caveolae in ventricular myocytes are required for stretch-dependent conduction slowing. *J Mol Cell Cardiol*, **76**: 265-274, 2014.
  20. Nagueh, SF: Mechanical dyssynchrony in congestive heart failure: diagnostic and therapeutic implications. *J Am Coll Cardiol*, **51**: 18-22, 2008.

21. Potse, M, Krause, D, Kroon, W, Murzilli, R, Muzzarelli, S, Regoli, F, Caiani, E, Prinzen, FW, Krause, R, Auricchio, A: Patient-specific modelling of cardiac electrophysiology in heart-failure patients. *Europace*, **16 Suppl 4**: iv56-iv61, 2014.
22. Arevalo, HJ, Vadakkumpadan, F, Guallar, E, Jebb, A, Malamas, P, Wu, KC, Trayanova, NA: Arrhythmia risk stratification of patients after myocardial infarction using personalized heart models. *Nat Commun*, **7**: 11437, 2016.
23. Augustin, CM, Neic, A, Liebmann, M, Prassl, AJ, Niederer, SA, Haase, G, Plank, G: Anatomically accurate high resolution modeling of human whole heart electromechanics: A strongly scalable algebraic multigrid solver method for nonlinear deformation. *J Comp Phys*, **305**: 622-646, 2016.
24. Kang, WH, Cao, W, Graudejus, O, Patel, TP, Wagner, S, Meaney, DF, Morrison, B, 3rd: Alterations in hippocampal network activity after in vitro traumatic brain injury. *J Neurotrauma*, **32**: 1011-1019, 2015.
25. Mineev, IR, Musienko, P, Hirsch, A, Barraud, Q, Wenger, N, Moraud, EM, Gandar, J, Capogrosso, M, Milekovic, T, Asboth, L, Torres, RF, Vachicouras, N, Liu, Q, Pavlova, N, Duis, S, Larmagnac, A, Voros, J, Micera, S, Suo, Z, Courtine, G, Lacour, SP: Electronic dura mater for long-term multimodal neural interfaces. *Science*, **347**: 159-163, 2015.
26. Yu, Z, Graudejus, O, Lacour, SP, Wagner, S, Morrison, B, 3rd: Neural sensing of electrical activity with stretchable microelectrode arrays. *Conf Proc IEEE Eng Med Biol Soc*, **2009**: 4210-4213, 2009.
27. Lacour, SP, Chan, D, Wagner, S, Li, T, Suo, Z: Mechanisms of reversible stretchability of thin metal films on elastomeric substrates. *Appl Phys Lett*, **88**: 204103-204101-204103-204103, 2006.

28. Dhillon, PS, Gray, R, Kojodjojo, P, Jabr, R, Chowdhury, R, Fry, CH, Peters, NS: Relationship between gap-junctional conductance and conduction velocity in mammalian myocardium. *Circ Arrhythm Electrophysiol*, **6**: 1208-1214, 2013.
29. Jack, JJB, Noble, D, Tsien, RW: *Electric current flow in excitable cells*, Oxford, Clarendon Press, 1975.
30. Khoshfetrat Pakazad, S, Savov, A, Braam, SR, Dekker, R: A platform for manufacturable stretchable micro-electrode arrays. *Procedia Eng*, **47**: 817-820, 2012.
31. Poulin, A, Saygili Demir, C, Rosset, S, Petrova, TV, Shea, H: Dielectric elastomer actuator for mechanical loading of 2D cell cultures. *Lab Chip*, **16**: 3788-3794, 2016.
32. McComb, C, Carrick, D, McClure, JD, Woodward, R, Radjenovic, A, Foster, JE, Berry, C: Assessment of the relationships between myocardial contractility and infarct tissue revealed by serial magnetic resonance imaging in patients with acute myocardial infarction. *Int J Cardiovasc Imaging*, **31**: 1201-1209, 2015.
33. Cooklin, M, Wallis, WR, Sheridan, DJ, Fry, CH: Changes in cell-to-cell electrical coupling associated with left ventricular hypertrophy. *Circ Res*, **80**: 765-771, 1997.
34. Fast, VG, Kléber, AG: Microscopic conduction in cultured strands of neonatal rat heart cells measured with voltage-sensitive dyes. *Circ Res*, **73**: 914-925, 1993.
35. Shaw, RM, Rudy, Y: Ionic mechanisms of propagation in cardiac tissue. Roles of the sodium and L-type calcium currents during reduced excitability and decreased gap junction coupling. *Circ Res*, **81**: 727-741, 1997.
36. Spach, MS, Heidlage, JF, Dolber, PC, Barr, RC: Electrophysiological effects of remodeling cardiac gap junctions and cell size: experimental and model studies of normal cardiac growth. *Circ Res*, **86**: 302-311, 2000.
37. Michela, P, Velia, V, Aldo, P, Ada, P: Role of connexin 43 in cardiovascular diseases. *Eur J Pharmacol*, **768**: 71-76, 2015.

38. Sundnes, J, Lines, GT, Cai, X, Nielsen, BF, Mardal, KA, Tveito, A: *Computing the electrical activity in the heart*, Springer Berlin Heidelberg New York, 2006.
39. Zhang, H, Iijima, K, Huang, J, Walcott, GP, Rogers, JM: Optical mapping of membrane potential and epicardial deformation in beating hearts. *Biophys J*, **111**: 438-451, 2016.
40. Zhuang, J, Yamada, KA, Saffitz, JE, Kleber, AG: Pulsatile stretch remodels cell-to-cell communication in cultured myocytes. *Circ Res*, **87**: 316-322, 2000.
41. Yu, JG, Russell, B: Cardiomyocyte remodeling and sarcomere addition after uniaxial static strain in vitro. *J Histochem Cytochem*, **53**: 839-844, 2005.
42. Boerboom, RA, Rubbens, MP, Driessen, NJ, Bouten, CV, Baaijens, FP: Effect of strain magnitude on the tissue properties of engineered cardiovascular constructs. *Ann Biomed Eng*, **36**: 244-253, 2008.
43. Hussain, W, Patel, PM, Chowdhury, RA, Cabo, C, Ciaccio, EJ, Lab, MJ, Duffy, HS, Wit, AL, Peters, NS: The renin-angiotensin system mediates the effects of stretch on conduction velocity, connexin43 expression, and redistribution in intact ventricle. *J Cardiovasc Electrophysiol*, **21**: 1276-1283, 2010.
44. Spach, MS, Miller, WT, 3rd, Dolber, PC, Kootsey, JM, Sommer, JR, Mosher, CE, Jr.: The functional role of structural complexities in the propagation of depolarization in the atrium of the dog. Cardiac conduction disturbances due to discontinuities of effective axial resistivity. *Circ Res*, **50**: 175-191, 1982.
45. de Bakker, JMT, Van Capelle, FJL, Janse, MJ, Tasseron, S, Vermeulen, JT, Dejonge, N, Lahpor, JR: Slow conduction in the infarcted human heart: zigzag course of activation. *Circulation*, **88**: 915-926, 1993.
46. Rohr, S: Myofibroblasts in diseased hearts: new players in cardiac arrhythmias? *Heart Rhythm*, **6**: 848-856, 2009.

47. Fast, VG, Kléber, AG: Block of impulse propagation at an abrupt tissue expansion: evaluation of the critical strand diameter in 2- and 3-dimensional computer models. *Cardiovasc Res*, **30**: 449-459, 1995.
48. Weise, LD, Panfilov, AV: New mechanism of spiral wave initiation in a reaction-diffusion-mechanics system. *PLoS One*, **6**: e27264, 2011.
49. Weise, LD, Panfilov, AV: Emergence of spiral wave activity in a mechanically heterogeneous reaction-diffusion-mechanics system. *Phys Rev Lett*, **108**: 228104, 2012.
50. Norton, LA, Andersen, KL, Arenholt-Bindslev, D, Andersen, L, Melsen, B: A methodical study of shape changes in human oral cells perturbed by a simulated orthodontic strain in vitro. *Arch Oral Biol*, **40**: 863-872, 1995.
51. Beauchamp, P, Desplantez, T, McCain, ML, Li, W, Asimaki, A, Rigoli, G, Parker, KK, Saffitz, JE, Kleber, AG: Electrical coupling and propagation in engineered ventricular myocardium with heterogeneous expression of connexin 43. *Circ Res*, **110**: 1445-1453, 2012.
52. Kucera, JP, Prudat, Y, Marcu, IC, Azzarito, M, Ullrich, ND: Slow conduction in mixed cultured strands of primary ventricular cells and stem cell-derived cardiomyocytes. *Front Cell Dev Biol*, **3**: 58, 2015.
53. Prudat, Y, Kucera, JP: Nonlinear behaviour of conduction and block in cardiac tissue with heterogeneous expression of connexin 43. *J Mol Cell Cardiol*, **76**: 46-54, 2014.
54. Rohr, S, Flückiger-Labrada, R, Kucera, JP: Photolithographically defined deposition of attachment factors as a versatile method for patterning the growth of different cell types in culture. *Pflugers Arch*, **446**: 125-132, 2003.
55. Akaike, H: A new look at the statistical model identification. *IEEE Trans Autom Control*, **19**: 716-723, 1974.

- 
56. Kondratyev, AA, Ponard, JG, Munteanu, A, Rohr, S, Kucera, JP: Dynamic changes of cardiac conduction during rapid pacing. *Am J Physiol Heart Circ Physiol*, **292**: H1796-H1811, 2007.
  57. Shors, SM, Sahakian, AV, Sih, HJ, Swiryn, S: A method for determining high-resolution activation time delays in unipolar cardiac mapping. *IEEE Trans Biomed Eng*, **43**: 1192-1196, 1996.
  58. Duchateau, J, Potse, M, Dubois, R: Spatially coherent activation maps for electrocardiographic imaging. *IEEE Trans Biomed Eng*, **64**: 1149-1156, 2017.

## Legends to figures

### **Figure 1. Design of stretchable microelectrode arrays (sMEAs).**

(a) Schematic showing the general sMEA layout (light red), the gold film electrodes, interconnects, and contact pads (black) and the encapsulated central area of the array (transparent grey square). The markers for strain quantification (7x8 array of dots) are visible in the inset. (b) Scanning electron micrograph of the microstructured gold film evaporated on the PDMS. (c) Photograph of a complete sMEA illuminated from the side.

### **Figure 2. Patterned cardiac cell strands, stretching system and imaging of strain.**

(a) Schematic (left) and photograph (right) of the central area of a sMEA with two 600  $\mu\text{m}$  wide cardiac cell strands (light red) oriented along the x-axis. For the photograph, the medium and the culture cylinder were removed, and the preparation was dried with warm air to render it visible. (b) Phase contrast photomicrograph of a cardiac cell strand passing over a recording electrode (note the perforated hole in the encapsulation layer) and two neighbouring markers. (c): sMEA system with its culture chamber mounted on the motorized stages and interfaced with PCB connectors. (d) Image of an sMEA in its reference unstrained state (top left), upon 10% uniaxial strain in the x-direction (orthodromic, right) or the y-direction (paradromic, bottom). The coloured circles identify the detected markers. The cardiac cell strands are not visible in the presence of medium. Note the culture cylinder and the ground (circular wire). Bottom right: Overlay of the marker positions (yellow: reference; magenta: orthodromic; cyan: paradromic). The arrows illustrate the corresponding strain tensors.

**Figure 3. Immediate and progressive changes of conduction velocity  $\theta$  upon application and release of uniaxial strain.**

(a) Extracellular electrograms recorded from a strand of foetal murine cardiomyocytes during continuous pacing (cycle duration: 400 ms) in the reference unstretched state (left) and 4 seconds later, after the application of 10% orthodromic strain (middle). The right panel shows the corresponding activation profiles ( $\theta$  in the unstretched strand: 27.73 cm/s;  $\theta$  upon strain: 26.26 cm/s). (b) Time course of  $\theta$  in a paced strand (cycle duration: 800 ms) before, during and after three 10-second stretches applied every 2 min (left), one 1-min long stretch (middle), and one 5-min long stretch (right). The periods during which stretch was applied (5% orthodromic strain) are highlighted by a grey background. (c) Time course of  $\theta$  in a paced strand (cycle length: 400 ms) before, during and after the application of 5%, 8% and 10% orthodromic strain (top) and paradromic strain (bottom) for 1 min (grey background). The insets illustrate the time course of  $\theta$  just before, during, and just after the operation of the linear stages (each inset lasts 8 sec).  $\theta$  was fitted with exponential functions (purple) before and during stretch as well as after release (excluding the time during which the stages were operating). The green arrows denote the absolute change of  $\theta$ .

**Figure 4. Immediate change of conduction velocity upon application and release of uniaxial strain.**

(a) Normalized  $\theta$  upon stretch (left panels) and release (right panels) for uniaxial orthodromic (top panels) and paradromic strain (bottom panels) of increasing magnitude. (b) Relative change of  $\theta$  in the material reference frame vs. strain magnitude, for orthodromic/paradromic strain and for stretch/release. Error bars denote 95% confidence intervals. Data were fitted with linear functions. (c) Same analysis as in (b) after converting  $\theta$  from the material to the spatial reference frame based on the measured strains.

**Figure 5. Immediate effects of uniaxial strain on conduction velocity  $\theta$ .**

(a) Relative change of  $\theta$  normalized by the magnitude of uniaxial orthodromic and paradromic strain ( $N_{ortho}$  and  $N_{para}$ ) upon stretch (left) and release (right), for cultured strands of foetal mouse and neonatal rat cardiomyocytes. (b) Difference between  $N_{para}$  and  $N_{ortho}$  as estimate of  $f_{myo}$ , the relative contribution of myoplasmic resistance to total axial resistance. Error bars denote mean  $\pm$  standard deviation. Oblique lines connect measurements from the same preparation.

**Figure 6. Progressive slowing and acceleration of conduction upon stretch and release.**

Change in the slope of the exponential fits of normalized  $\theta$  vs. time (in %/min) upon stretch (left) and release (right), for orthodromic and paradromic strain and for strands of foetal mouse and neonatal rat cardiomyocytes. Error bars denote mean  $\pm$  standard deviation. Oblique lines connect measurements from the same preparation.

## Figures

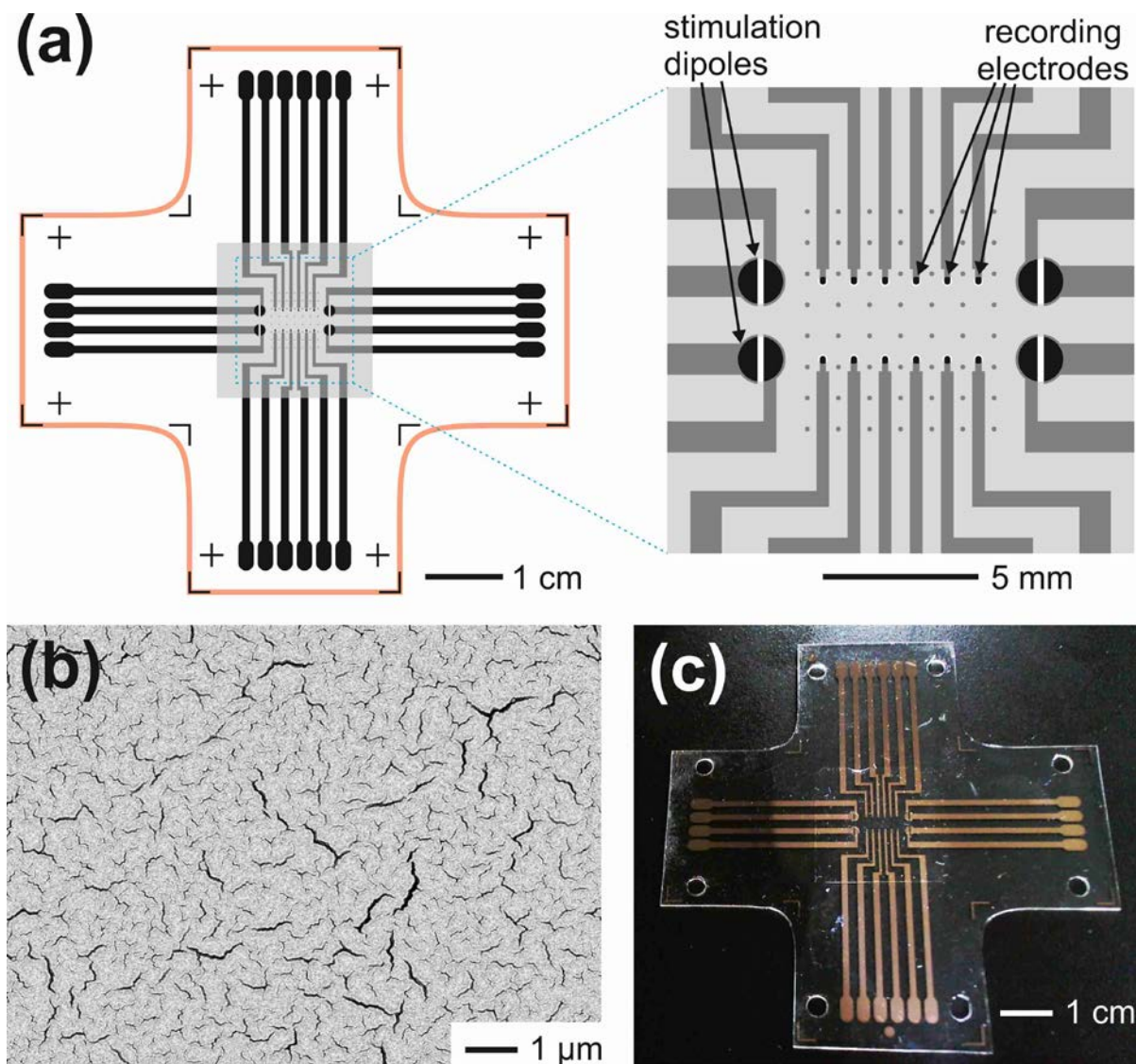


**Figure 1. Design of stretchable microelectrode arrays (sMEAs).**

(a) Schematic showing the general sMEA layout (light red), the gold film electrodes, interconnects, and contact pads (black) and the encapsulated central area of the array (transparent grey square). The markers for strain quantification (7x8 array of dots) are visible in the inset. (b) Scanning electron micrograph of the microstructured gold film evaporated on the PDMS. (c) Photograph of a complete sMEA illuminated from the side.

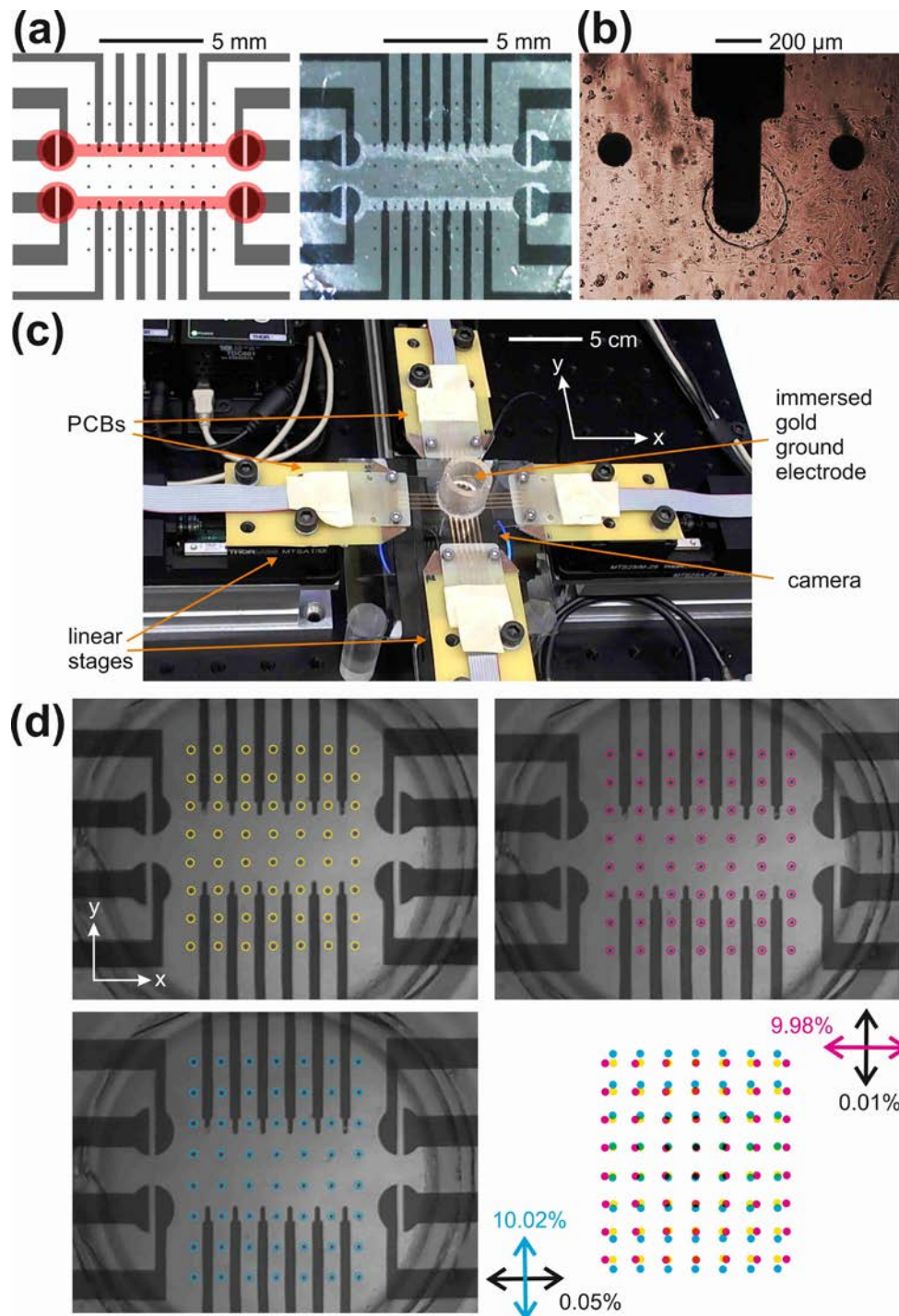


**Figure 2. Patterned cardiac cell strands, stretching system and imaging of strain.**

(a) Schematic (left) and photograph (right) of the central area of a sMEA with two 600 μm wide cardiac cell strands (light red) oriented along the x-axis. For the photograph, the medium and the culture cylinder were removed, and the preparation was dried with warm air to render it visible. (b) Phase contrast photomicrograph of a cardiac cell strand passing over a recording electrode (note the perforated hole in the encapsulation layer) and two neighbouring markers. (c) sMEA system with its culture chamber mounted on the motorized stages and interfaced with PCB connectors. (d) Image of an sMEA in its reference unstrained state (top left), upon 10% uniaxial strain in the x-direction (orthodromic, right) or the y-direction (paradromic, bottom). The coloured circles identify the detected markers. The cardiac cell strands are not visible in the presence of medium. Note the culture cylinder and the ground (circular wire). Bottom right: Overlay of the marker positions (yellow: reference; magenta: orthodromic; cyan: paradromic). The arrows illustrate the corresponding strain tensors.

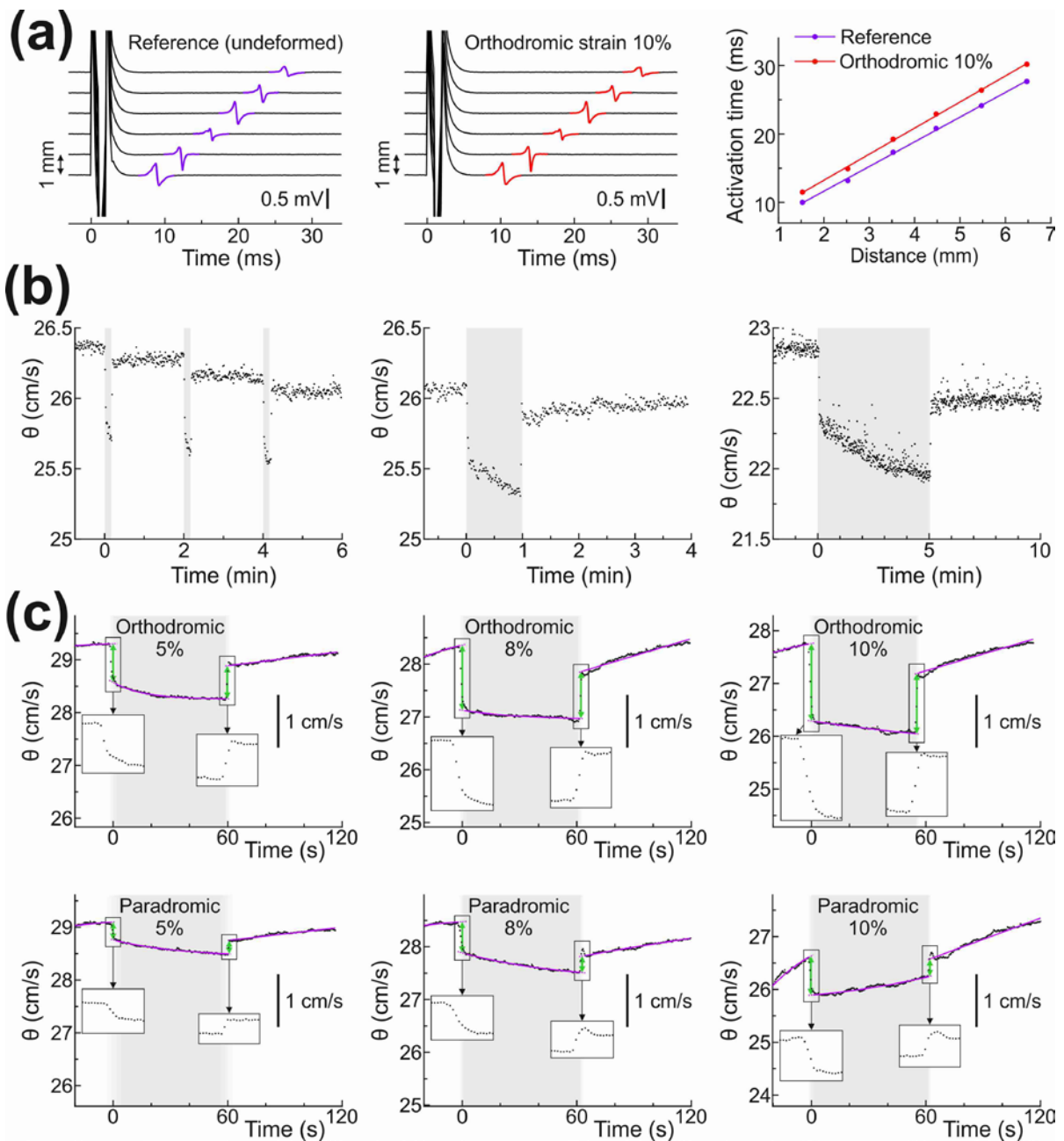


**Figure 3. Immediate and progressive changes of conduction velocity  $\theta$  upon application and release of uniaxial strain.**

(a) Extracellular electrograms recorded from a strand of foetal murine cardiomyocytes during continuous pacing (cycle duration: 400 ms) in the reference unstretched state (left) and 4 seconds later, after the application of 10% orthodromic strain (middle). The right panel shows the corresponding activation profiles ( $\theta$  in the unstretched strand: 27.73 cm/s;  $\theta$  upon strain: 26.26 cm/s). (b) Time course of  $\theta$  in a paced strand (cycle duration: 800 ms) before, during and after three 10-second stretches applied every 2 min (left), one 1-min long stretch (middle), and one 5-min long stretch (right). The periods during which stretch was applied (5% orthodromic strain) are highlighted by a grey background. (c) Time course of  $\theta$  in a paced strand (cycle length: 400 ms) before, during and after the application of 5%, 8% and 10% orthodromic strain (top) and paradromic strain (bottom) for 1 min (grey background). The insets illustrate the time course of  $\theta$  just before, during, and just after the operation of the linear stages (each inset lasts 8 sec).  $\theta$  was fitted with exponential functions (purple) before and during stretch as well as after release (excluding the time during which the stages were operating). The green arrows denote the absolute change of  $\theta$ .

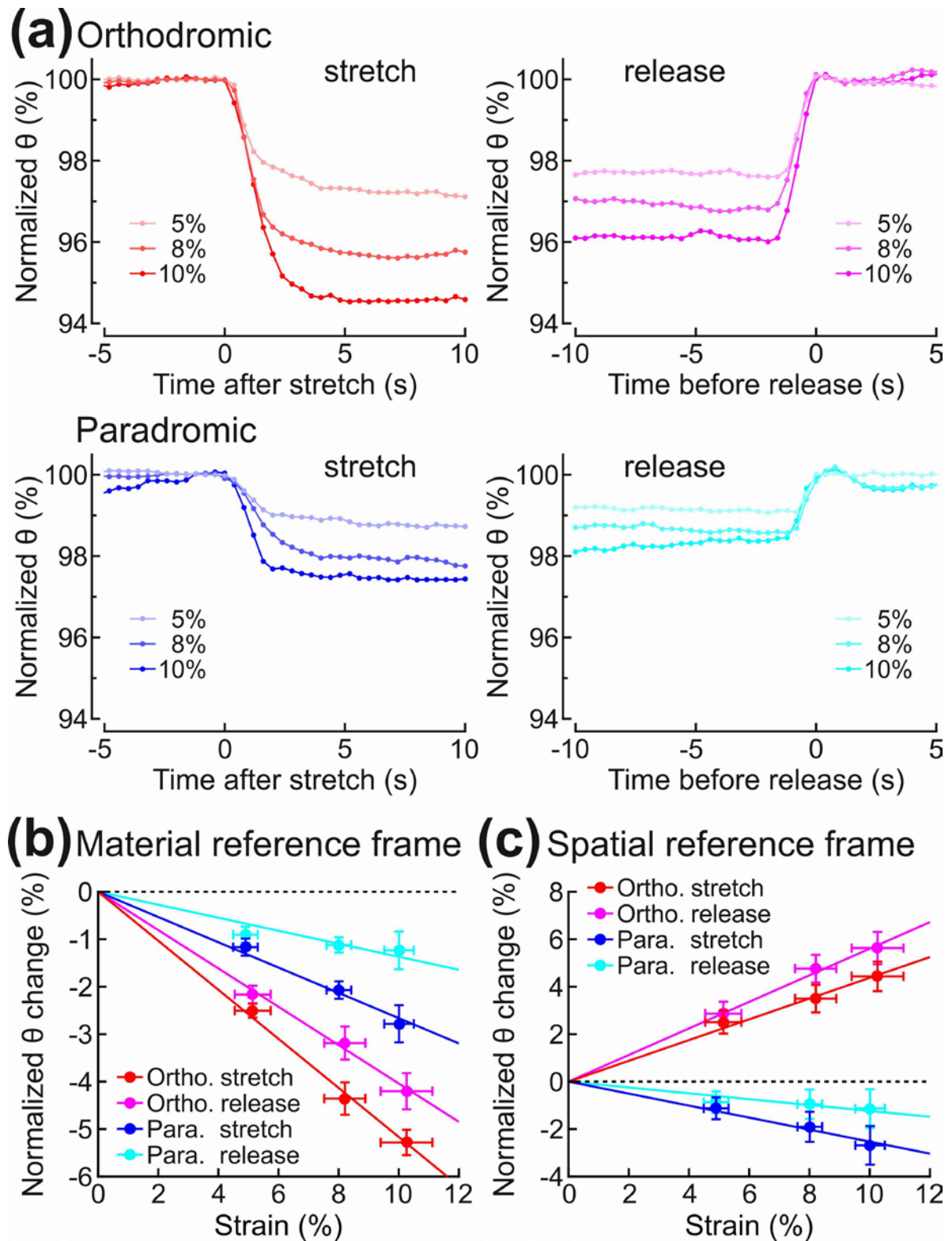


**Figure 4. Immediate change of conduction velocity upon application and release of uniaxial strain.**

(a) Normalized  $\theta$  upon stretch (left panels) and release (right panels) for uniaxial orthodromic (top panels) and paradromic strain (bottom panels) of increasing magnitude. (b) Relative change of  $\theta$  in the material reference frame vs. strain magnitude, for orthodromic/paradromic strain and for stretch/release. Error bars denote 95% confidence intervals. Data were fitted with linear functions. (c) Same analysis as in (b) after converting  $\theta$  from the material to the spatial reference frame based on the measured strains.

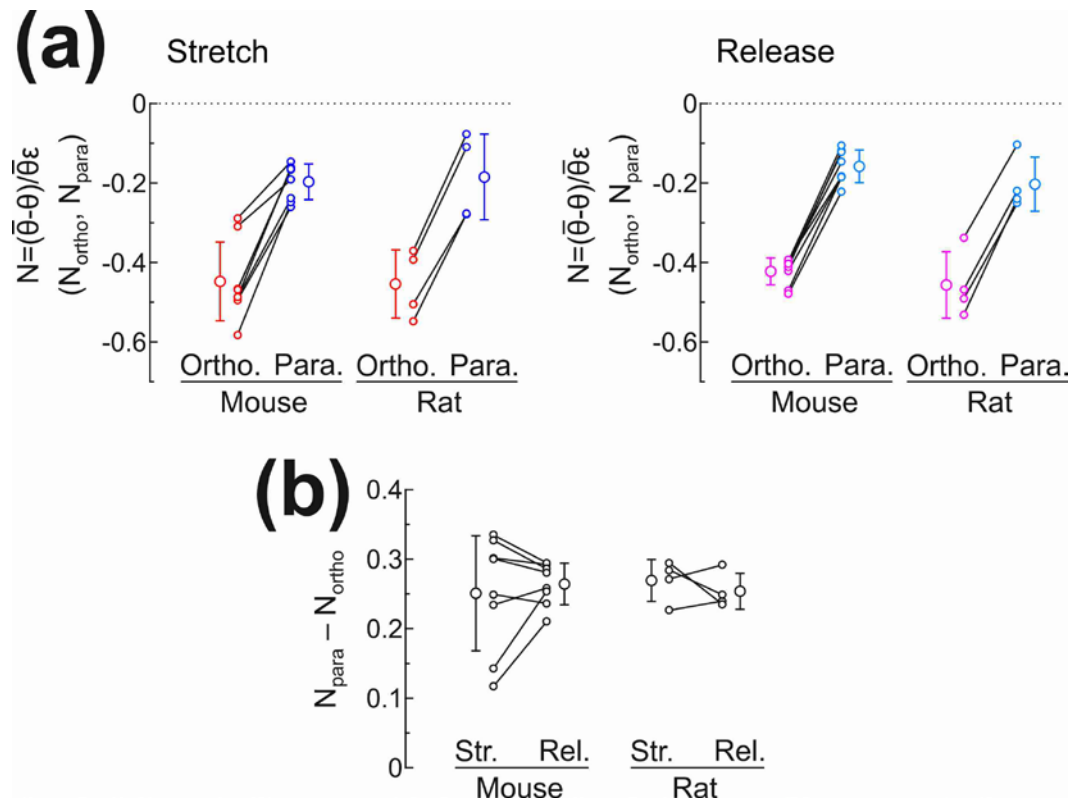


**Figure 5. Immediate effects of uniaxial strain on conduction velocity  $\theta$ .**

(a) Relative change of  $\theta$  normalized by the magnitude of uniaxial orthodromic and paradromic strain ( $N_{ortho}$  and  $N_{para}$ ) upon stretch (left) and release (right), for cultured strands of foetal mouse and neonatal rat cardiomyocytes. (b) Difference between  $N_{para}$  and  $N_{ortho}$  as estimate of  $f_{myo}$ , the relative contribution of myoplasmic resistance to total axial resistance. Error bars denote mean  $\pm$  standard deviation. Oblique lines connect measurements from the same preparation.

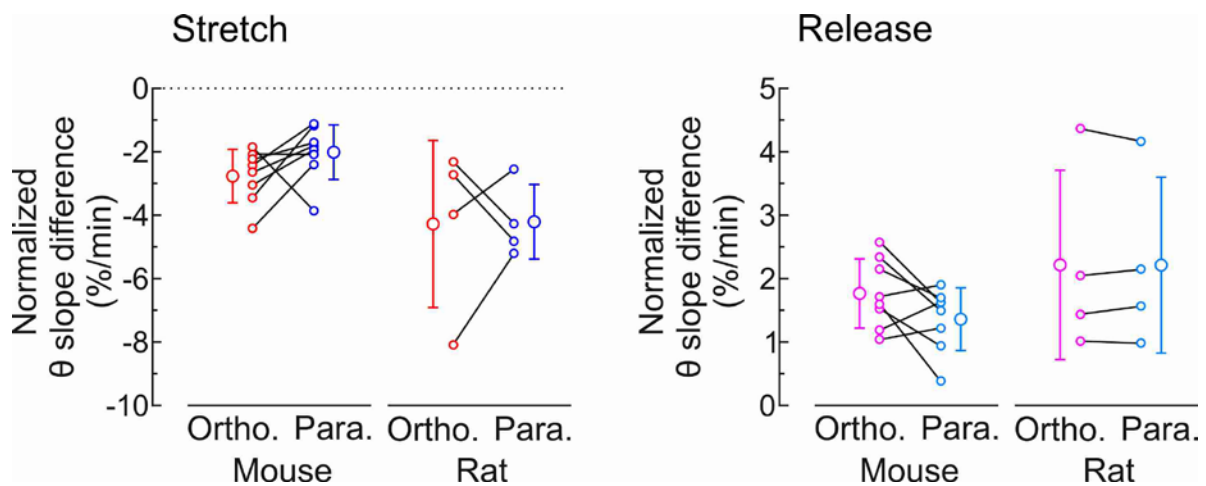


**Figure 6. Progressive slowing and acceleration of conduction upon stretch and release.**

Change in the slope of the exponential fits of normalized  $\theta$  vs. time (in %/min) upon stretch (left) and release (right), for orthodromic and paradromic strain and for strands of foetal mouse and neonatal rat cardiomyocytes. Error bars denote mean  $\pm$  standard deviation. Oblique lines connect measurements from the same preparation.

## Physiological relevance

In the heart, the velocity of action potential propagation is an important electrophysiological parameter. Slow conduction is crucial in the generation of potentially life-threatening heart rhythm disturbances. Conduction velocity is determined by numerous factors, including the function of ion channels, the resistances of the myoplasm, the gap junctions and the extracellular space and the electrical capacitance of the membrane. These properties can be influenced by changes in the shape of cardiac muscle, e.g., by stretch. Thus, deformation of the myocardium exerts a feedback on its electrical properties, called mechano-electrical feedback. Using recent technologies, we developed stretchable microelectrode arrays on which we cultured strands of cardiac cells. These arrays were mounted in a setup permitting to apply controlled stretches to these preparations in the direction of propagation or perpendicular to it. We found that stretch in the direction of action potential propagation slows propagation more than stretch in the perpendicular direction. Based on cable theory, this stronger effect is due to an increase of myoplasmic resistance. Thus, not only the magnitude of cardiac tissue deformation but also the direction of this deformation relative to propagation is determinant in the generation of slow conduction and, in the diseased heart, of arrhythmias. Our findings are important for a comprehensive understanding of mechano-electrical feedback and of arrhythmias in general, and we believe that the mechanisms that we report should be incorporated into modern computational models of the contracting heart, which can be tailored to individual patients and thus bear promise for personalized medicine.